Numerical simulation of dispersion around an isolated cubic building: Model evaluation of RANS and LES

Yoshihide Tominaga[a] and Ted Stathopoulos[b]

[a]*Department of Architecture and Building Engineering, Niigata Institute of Technology, 1719 Fujihashi, Kashiwazaki, Niigata, 945-1195, Japan,*
[b]*Centre for Building Studies, Department of Building, Civil and Environmental Engineering, Concordia University, 1455 de Maisonneuve Blvd West, H3G 1M8, Montreal, Quebec, Canada*
* Corresponding author: Tel&Fax: 81-257-22-8176, E-mail : tominaga@abe.niit.ac.jp (Y. Tominaga)

Abstract

Several studies have been carried out on CFD prediction based on a RANS (Reynolds Averaged Navier-Stokes equations) model for dispersion around buildings, but it was reported that a RANS computation often provides extremely high concentration, which are not observed in usual measurements. These results suggest that transient simulations such as the large-eddy simulation (LES) might be required to achieve more accurate results. Nevertheless, very few studies have evaluated the basic performance of LES in modeling the dispersion field for a simple configuration in comparison with the RANS model. Therefore, relative performance of these simulation methods for dispersion problem around buildings should be clarified in order to make it possible to choose a suitable numerical method for its purpose. The purpose of this study is to confirm the accuracy of LES in modeling plume dispersion near and around a simple building model and to clarify the mechanism for the discrepancy in relation to the RANS computation. Simple LES modeling gives better results than RNG modeling of the distribution of concentration, although the difference for mean velocity is not so large. The horizontal diffusion of concentration is well reproduced by LES. This tendency is closely related to the reproduction of unsteady periodic fluctuation around cubical forms in LES.

Keywords

1 Introduction

Prediction of plume dispersion near buildings is very important for the design of exhaust vents and air intakes to avoid adverse air quality impacts. Several studies have been carried out on CFD prediction based on a RANS (Reynolds Averaged Navier-Stokes equations) model for dispersion around buildings [1-3], but it was reported that a RANS computation often provides extremely high concentration, which are not observed in usual measurements. Here it should be pointed out that lower concentrations can be predicted in specified cases by the pseudo-diffusivity which often appears in RANS computations with coarse grid spacing. Recently, the authors have examined the performance of various revised k-ε models for the dispersion field around a building and confirmed that all RANS computations under-predicted the horizontal concentration diffusion, although some revised k-ε models yielded much more accurate results than the standard k-ε model [4]. The same tendency was pointed out by Blocken et al. [5] through steady-state RANS computations of pollutant dispersion in the neutrally stable atmospheric boundary layer for several case studies. The study concluded that transient simulations might be required to achieve more accurate results.

It is well known that in contrast to RANS the large-eddy simulation (LES) resolves large-scale unsteady motions and requires modeling only of the small-scale. Therefore, the dynamic character such as fluctuations of wind pressure on buildings, which are primarily due to large-scale motions, can be reproduced in LES [6-8]. Furthermore, several studies have argued that the results of LES show good agreement with the experiment in terms of the distributions of mean velocity and turbulence energy around a simple building, even when the simplified sub-grid scale model was used [9-11]. This is because the momentum diffusion due to vortex shedding around the building, which is not reproduced in steady-state RANS computation, is closely related to the formation of the mean flowfield. Of course, LES requires larger computational resources and presently it is recognized as a research tool rather than as an instrument to solve practical cases of interest. However, it has become a versatile modeling tool that can be applied to more complicated practical problems for collecting more

detailed information about the transient turbulent flow with the rapid development of computer hardware and numerical methodologies [12, 13]. Therefore, relative performance of these simulation methods for dispersion problem around buildings should be clarified in order to make it possible to choose a suitable numerical method for its purpose. Nevertheless, very few studies have evaluated the basic performance of LES in modeling the dispersion field for a simple configuration in comparison with the RANS model. Previous studies on LES regarding dispersion of exhaust around a building focused mainly on distributions of concentration in the wake region behind a building [14, 15]. However, concentrations on building surfaces are closely related to the design of exhaust vents and air intakes particularly when exhaust contains toxic, flammable or odorous components. Thus LES, which can evaluate peak values for concentration may have great advantages compared to the RANS approach.

The purpose of this study is to confirm the accuracy of LES in modeling dispersion near and around a simple building model and to clarify the mechanism of the discrepancy in relation to the RANS computation.

2 Computational details

2.1 Flow field

The flow field selected as a test case was that around a cubic building with a flush vent at the rooftop placed within the neutral surface boundary layer (cf. Fig. 1). First, the wind tunnel measurements of velocity around a cubic model without vent emission carried out for this study by the authors were used for validation of the prediction accuracy of velocity field by CFD (Flow I). In this experiment, wind velocity was measured by a split fibre probe, which can discern three-dimensional components of velocity vector. The Reynolds number based on H_b and $<u_b>$ was 6.4×10^4 (H_b is the cube height and $<u_b>$ is the mean inlet velocity at H_b; hereafter $<>$ denotes a time-averaged value). Then, the wind tunnel measurements by Li and Meroney [16] were used for the comparison in the concentration field with vent emission (Flow II). The Reynolds number based on H_b and $<u_b>$ was 1.1×10^4. The turbulence intensity levels of two experiments are almost same. The case of a central roof vent with 0º wind direction is adopted in this study. The ratio of the exit velocity, W_S to $<u_b>$ was 0.19. Thus, the plume was likely trapped in the recirculation zone on the roof, as opposed to most previous plume dispersion studies [5, 17, 18, 19] conducted with a significant exhaust velocity. On the other hand, the influence of the exit velocity on the flow field around the cube is much smaller in the present study, so the exhaust conditions are more realistic than those in previous cases.
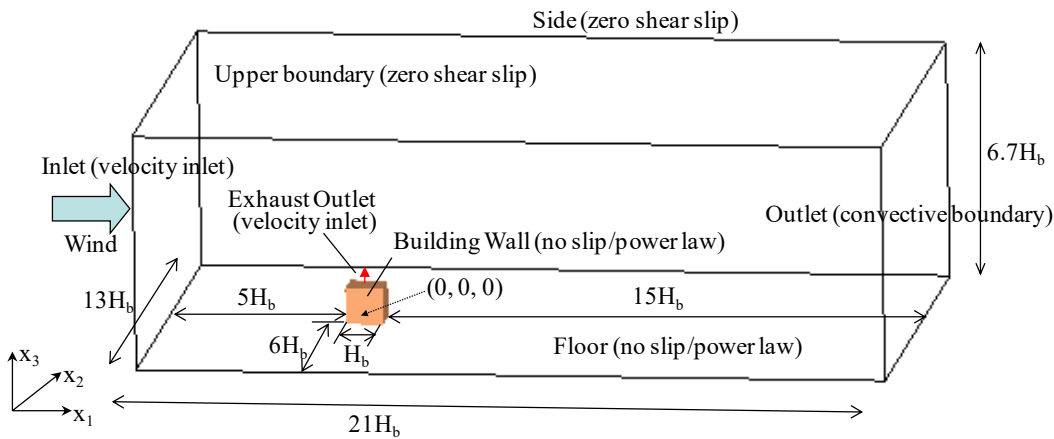

Fig. 1. Computational domain and boundary conditions (LES).

2.2 Numerical methods

The self-developed code used for the calculations is based on a finite volume approach for solving the flow and concentration equations on structured rectangular grids in both computations.

1) RANS
The RNG k-ε model [20] (hereafter RNG), which shows best agreement with the experiment of the four types of turbulence models in the previous study [4], was used. The turbulent Schmidt number was set to 0.7 [21]. The QUICK scheme was used for discretizing momentum and concentration equations. Unsteady calculations were

carried out, but results obtained by RNG showed almost no vortex shedding.

2) LES

The standard Smagorinsky model [22] with the empirical constant C_S=0.12 was used for the sub-grid scale eddy viscosity model [9]. A dynamic procedure [14, 23] is often used as sub-grid scale model in recent LES computations. However, the dynamic type model tends to cause numerical instability and take a large computational time. Moreover, a discrepancy of near-wall behavior in the dynamic type LES applied to three-dimensional flow has been reported [24]. Considering this situation, the simple and traditional sub-grid scale model was used in order to focus on only the difference of the modeling approach between RANS and LES, that is, whether transient flow can or cannot be solved. Near the wall, the length scale is modified by a van Driest damping function. The sub-grid scale Schmidt number was set to 0.5 [25]. A second-order centered difference scheme is adopted for the spatial derivatives. For time advancement, the Adams-Bashforth scheme is used for the convection terms and the Crank-Nicolson scheme for the diffusion terms. The computations were conducted for 132 non-dimensional time units t^* ($=t \times <u_b>/H_b$) to determine the time averaged values.

2.3 Boundary conditions

The computational domain and boundary conditions are summarized in Fig. 1. This domain was discretized into $86(x_1) \times 76(x_2) \times 46(x_3)$ grids. The minimum grid width was $0.0045H_b$. These conditions are the same in both computations. In the RNG case, it was confirmed that the prediction results did not change significantly with the finer grids as reported in [4]. In order to evaluate the accuracy of the LES computation including the effect of grid dependence, identical (with the RNG case) grids were used. Turbulence in the exhaust outlet velocity was not considered in either case.

1) RNG

The vertical distributions of $<u_1>$, k and ε at the inflow boundaries were based on the experiment. The generalized log law [26] was used for the solid boundary. The details of the boundary conditions used are provided by Tominaga and Stathopoulos (2009).

2) LES

A separate LES computation of turbulent boundary layer flow was conducted to generate inflow turbulence. The inflow generating method used here was that proposed by Kataoka and Mizuno [27]. Fig. 2 compares the profiles of mean velocity $<u_1>$ and turbulence intensity (Ix_1) in streamwise components at the end of a driver section with the experimental values. The computation accurately reproduced the turbulence property of the inflow condition in the experiment. The little disagreement of the turbulence intensity at $x_3>3H_b$ was caused by the fact that the velocity fluctuation at the upper region was much suppressed by the damping function used here. The same tendency was reported in the previous research using this method [27, 28]. For the boundary condition at the solid walls, a linear or 1/7 power law distribution of instantaneous velocity was assumed [29]. This condition is based on an explicit power-law approximation to the log-law outside interfaced with the linear profile inside the viscous sub-layer. It was confirmed that most of first grid points adjacent to the wall boundary were located in the viscous sub-layer in this computation. This means that no-slip boundary condition was applied to most of the solid surfaces.
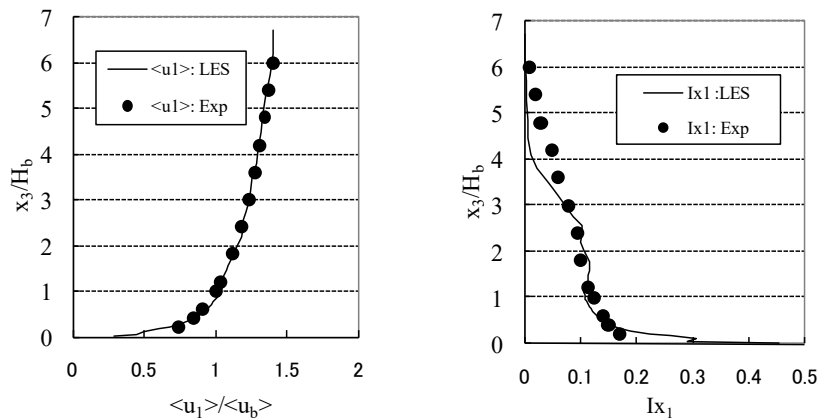
(1) Time-averaged streamwise velocity   (2) Turbulence intensity in streamwise direction

Fig. 2. Inflow profiles obtained by computations in driver region in LES.

3 Results and Discussion

3.1 *Flow fields without vent emission (Flow I)*

Firstly, the velocity fields without vent emission (Flow I) obtained by RNG and LES computations were determined. The results were compared with the experimental data for the same configuration obtained by the authors, because there were no data of velocity around the cube in Li and Meroney [16]. The computations were conducted with the boundary condition corresponding to the author's experiment.

Table 1 compares the reattachment lengths on the roof (X_R) and behind the building (X_F). The X_R values obtained by both computations show good agreement with the experimental values, although the value obtained by RNG is slightly larger than the experimental value. On the other hand, X_F is greatly overestimated in RNG as also pointed out in the previous study [11], while this discrepancy is much improved in LES. Fig. 3 shows the profiles of streamwise velocities on the roof and downstream of the cube at the centerline. The differences between the velocity distributions of the two models were rather small, but the reverse flows on the roof and behind the cube in RNG were somewhat larger than those in LES as mentioned earlier. This means that the mixing effect near the cube in LES was stronger than that in RNG.

Table 1 Comparison of reattachment lengths on roof and behind cube

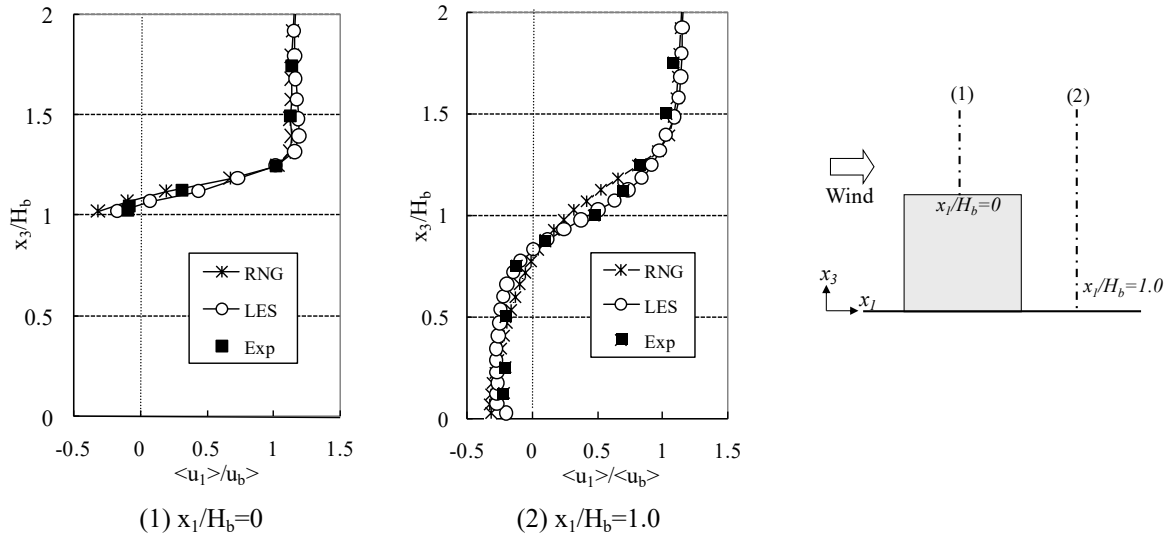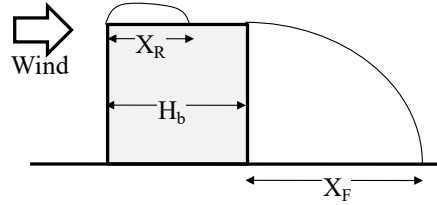|	X_R	X_F
RNG	$0.87H_b$	$2.46H_b$
LES	$0.79H_b$	$1.54H_b$
Experiment	$0.64H_b$	$1.33H_b$

(1) $x_1/H_b=0$ (2) $x_1/H_b=1.0$

Fig. 3. Comparison of vertical distribution of streamwise velocity on roof and downstream of cube at centerline.

3.2 *Flow fields with vent emission (Flow II)*

Fig. 4 compares the velocity vectors on the roof and walls with vent emission under the boundary condition provided by Li and Meroney [16] (Flow II). The effect of vent emission on the velocity field is rather small. The reverse flow on the roof in RNG is concentrated more to the centerline than that in LES, that is, larger turbulence mixing occurs in LES. The reverse flows on the leeward and side walls obtained by RNG are somewhat larger than those by LES.

The distributions of k on the roof and downstream of the cube at the centerline are illustrated in Fig. 5. The

4

value of k given by LES is larger than that given by RNG except in the region behind the cube. Peaks of k above the roof are observed in both models, but they are much larger in LES than in RNG. This smaller value of k in RNG is closely related to the stronger reverse flow on the roof in this model than that given by LES. Fig. 6 shows the distributions of k near the roof and the wall surfaces. The distribution patterns of k in the two models are completely different. A large value of k appears at the edge of the frontal edge of the cube in RNG, while in LES two symmetrical peaks are observed in the upstream region of the roof where the recirculation flow exists (cf. Fig. 4).
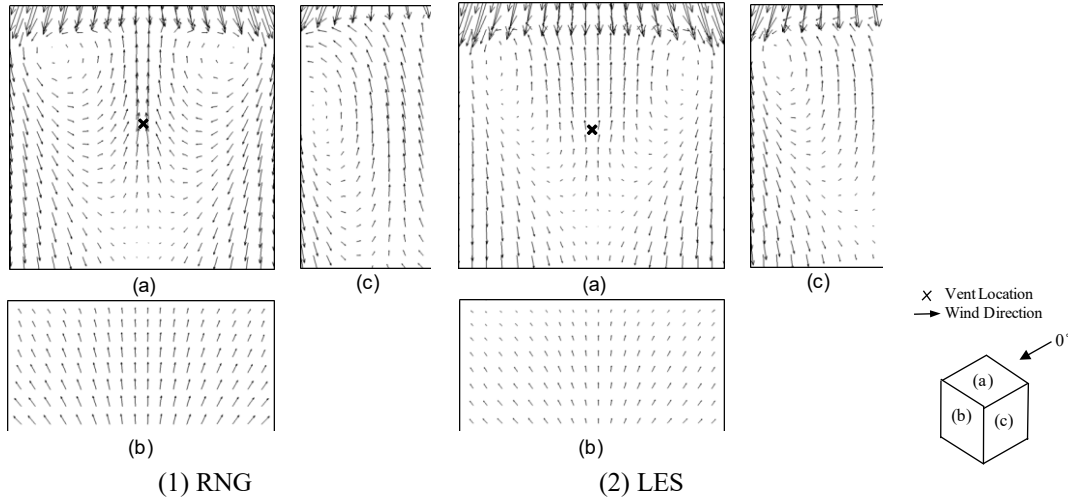

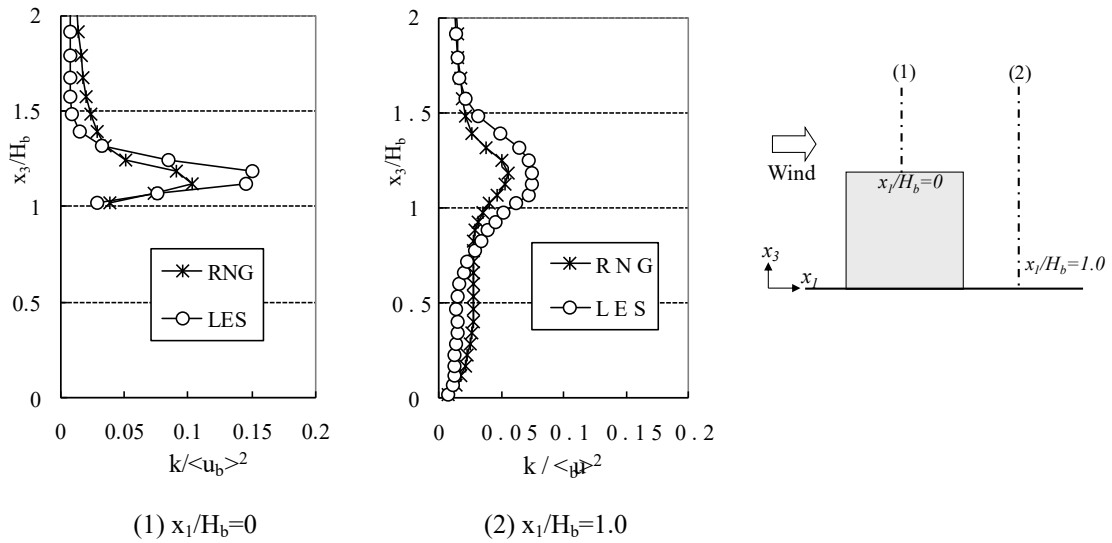Fig. 4. Comparison of velocity vectors on roof and wall surfaces.

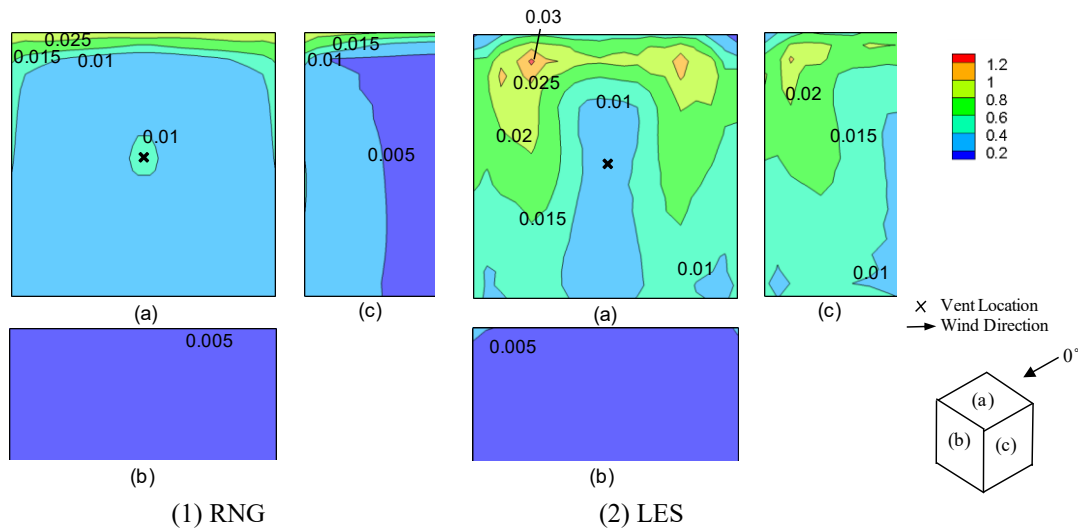Fig. 5. Comparison of vertical distribution of k on roof and downstream of cube at centerline.

5

Fig. 6. Contours of turbulent energy k on roof and wall surfaces.

3.3 Time-averaged concentration

Fig. 7 compares the contours of the time-averaged dimensionless concentration, $<K>$, on the roof and wall surfaces obtained from the present CFD and the experiment by Li and Meroney [16]. In this study, dimensionless concentration $<K>$ was defined as $<K>=<c>/<c_0>$, where $<c_0>=Q_e/H_b^2<u_b>$, $<c>$ is mean concentration and Q_e is the plume flow rate. On the roof surface, the high concentration region ($K>100$) upwind of the vent in RNG was larger than those in LES and the experiment. The contours of K in RNG also expand greatly in the upstream direction. Generally, RNG underestimates the turbulence diffusion around the cube. This is why the smaller value of turbulent Schmidt number worked well in the previous studies [4, 5, 21]. On the other hand, the concentrations are widely spread in the horizontal direction in LES. The general distribution of $<K>$ given by LES is very similar to that of the experiment, although the LES result tends to be a little diffusive. At the side and leeward wall surfaces, the distribution patterns are much different in the two models, and RNG shows smaller values of concentration than LES. The concentrations at the side wall in RNG are mainly transferred from the leeward direction by the recirculation flow (cf. Fig. 4(1)), although those in LES are coming from the roof as in the experiment.

The distribution of $<K>$ on the centerline of the roof and walls is shown in Fig. 8. Another experimental result with the central vent release for the same configuration by Saathoff et al. [30] was also compared for reference. In the streamwise direction, the values of $<K>$ given by LES are smaller than those given by RNG. However, in the lateral direction, the LES values are much higher than the RNG values and near the experimental data. In general, the distributions of $<K>$ obtained by LES show very good agreement. These results are caused by larger lateral turbulence diffusion obtained by LES in comparison with RNG. The vertical distributions of time-averaged concentration $<K>$ at the center section of the cube are shown in Fig. 9. The high concentration region above the roof in RNG is advected more to the downwind than that in LES. Therefore, the ground-level concentration behind the cube in RNG becomes higher. In contrast, the concentration above the roof in LES is spread to vertical direction due to a larger mixing effect than that of RNG. Fig. 10 indicates the contours of dimensionless concentration $<K>$ in the near wake region ($x_1/H_b=1.0$). RNG under-predicts the horizontal spread of concentration in comparison with the experiment. However, LES shows better prediction of diffusivity of horizontal concentration, although the vertical diffusion is slightly over-predicted.
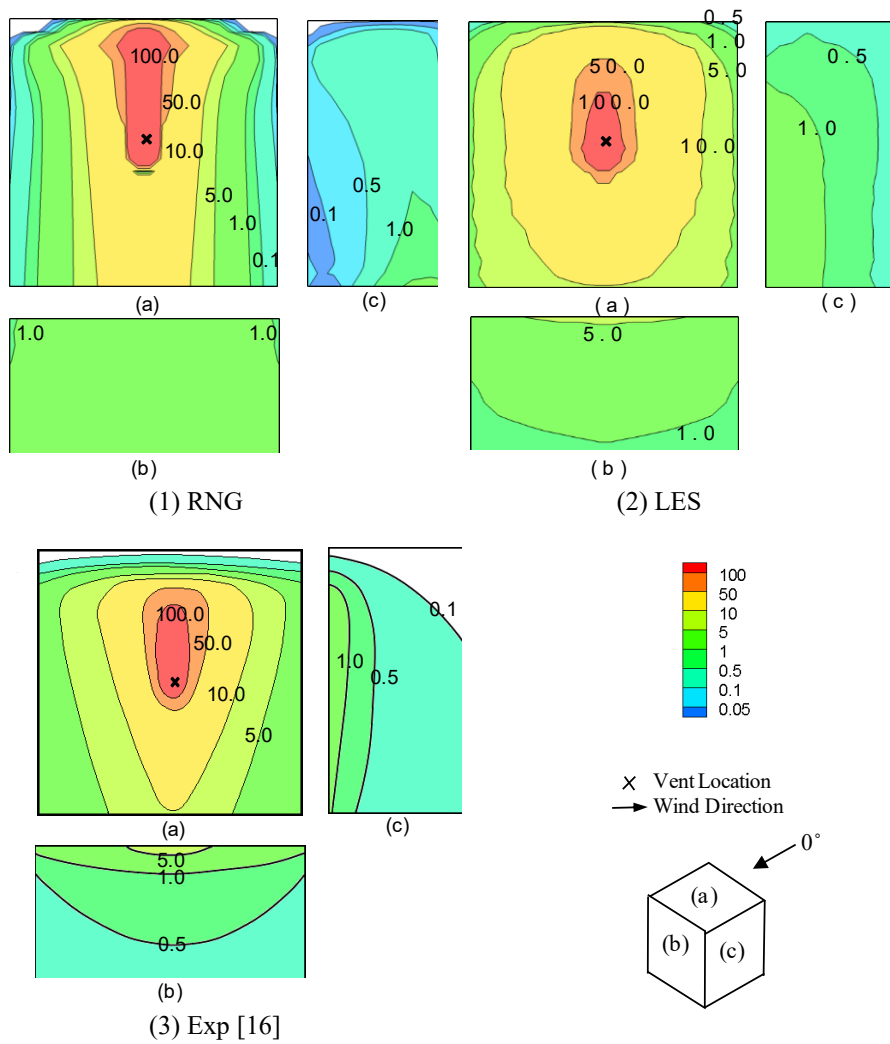
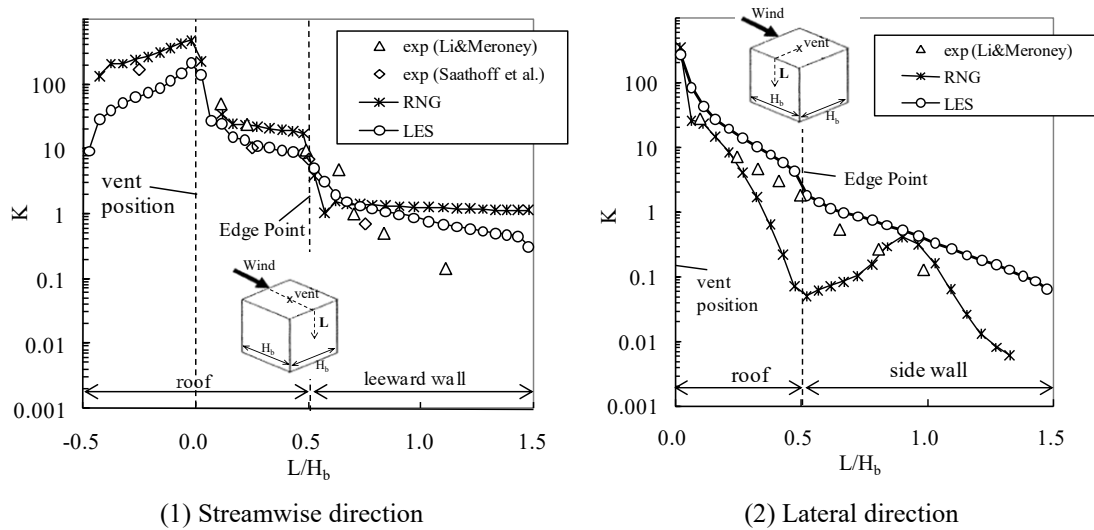Fig. 7. Distribution of time-averaged dimensionless concentration <K> on roof and wall surfaces.

(1) Streamwise direction

(2) Lateral direction

Fig. 8. Distribution of time-averaged dimensionless concentration <K> on centerline of roof, leeward and side wall.

| (1) RNG | (2) LES |

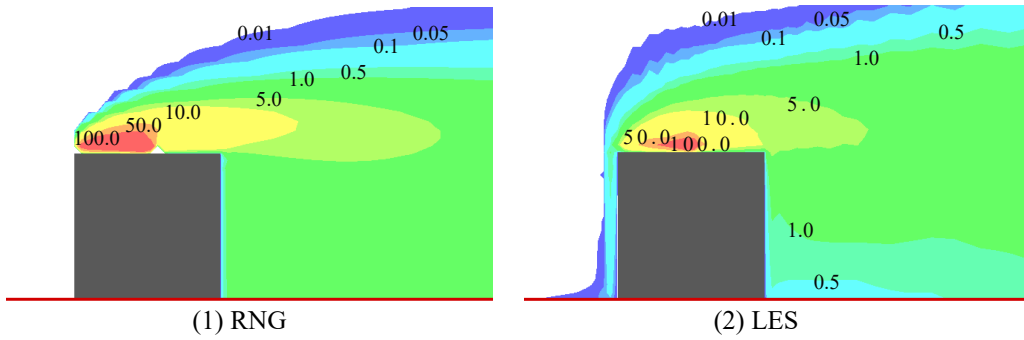Fig. 9. Contours of time-averaged dimensionless concentration <K> at center section.
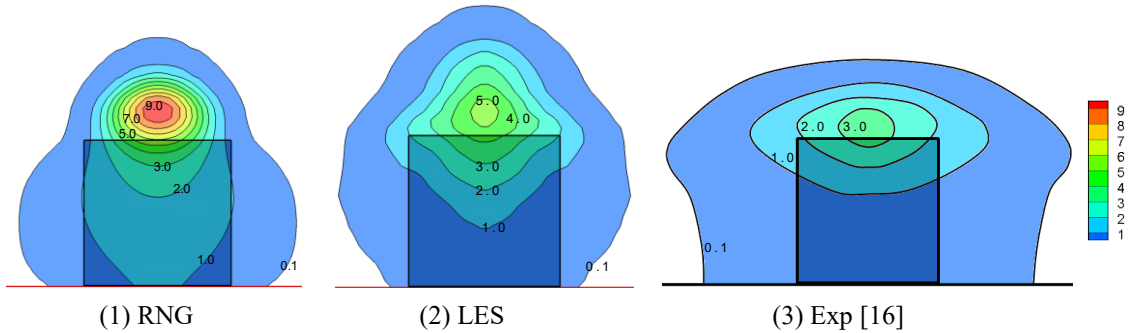

| (1) RNG | (2) LES | (3) Exp [16] |

Fig. 10. Contours of time-averaged dimensionless concentration <K> in near wake region (x_1/H_b=1.0).

3.4   Concentration fluxes

The distribution of concentration fluxes represents the essentials of concentration transport; it can provide very important information to investigate the validity of a model used for concentration transport. Scalar transport of concentration consists of convective and turbulent diffusion effects, which are expressed by the convection as the mean scalar fluxes <u_i><c> and the turbulent diffusion fluxes <u_i'c'>, respectively. The convective fluxes can be estimated by using mean velocities <u_i> and mean concentration <c>. Although the turbulent diffusion fluxes are calculated directly in LES, they are modeled by the gradient diffusion hypothesis, $-<u_i'c'>=\dfrac{v_t}{Sc_t}\dfrac{\partial<c>}{\partial x_i}$, where v_t is the eddy viscosity and Sc_t is the turbulent Schmidt number, in RNG.

Fig. 11 compares the streamwise components of the convective flux <u_1><c> and the turbulent diffusion flux <u_1'c'> along the centerline on the roof. The negative value of <u_1><c> at upwind region of the vent in RNG is much larger than that in LES, because the reverse flow on the roof in RNG is stronger than that in LES, as shown in Fig. 4. On the other hand, the turbulent diffusion flux <u_1'c'> at upwind region of the vent in LES shows a larger value than that in RNG, although the absolute values in both models are rather small in comparison with the convective flux. The LES result shows a large positive peak behind the vent position, which is very small in RNG.

The lateral components of convective flux <u_2><c> and turbulent diffusion flux <u_2'c'> along the line across the vent are shown in Fig. 12. The peaks of convective flux, <u_2><c>, which show opposite signs in the two models, are observed on the sides of the vent position. This is because the flow directions in this area are different in the two models (cf. Fig. 4). Furthermore, a large difference between the two models is observed in the distribution of turbulent diffusion flux <u_2'c'>. The result of RNG shows two sharp peaks in the area adjacent to the vent position, which gives opposite signs to the peaks of the convective flux obtained by this model. These lateral component fluxes are canceled in RNG. By contrast, in LES, large values of flux are widely spread in the lateral directions with the same signs in two fluxes. Consequently, LES shows a much larger contribution of the turbulent diffusion fluxes than RNG. Judging from the good agreement with the experimental data in terms of mean concentration distributions as shown in Figs. 7 and 8, it appears that the concentration fluxes obtained by LES reproduce the actual behavior of concentration transport. The large difference between the modeled turbulent fluxes suggests that the accuracy of turbulent diffusion modeling is very important in predicting the mean concentration distribution.
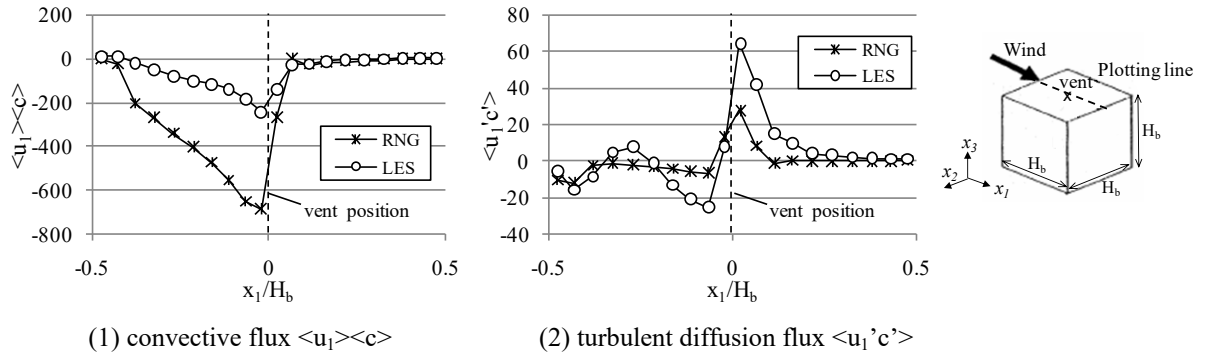
(1) convective flux $\langle u_1 \rangle \langle c \rangle$ (2) turbulent diffusion flux $\langle u_1'c' \rangle$

Fig. 11. Comparison of streamwise components of convective flux $\langle u_1 \rangle \langle c \rangle$ and turbulent diffusion flux $\langle u_1'c' \rangle$ on roof.

(1) convective flux $\langle u_2 \rangle \langle c \rangle$ (2) turbulent diffusion flux $\langle u_2'c' \rangle$
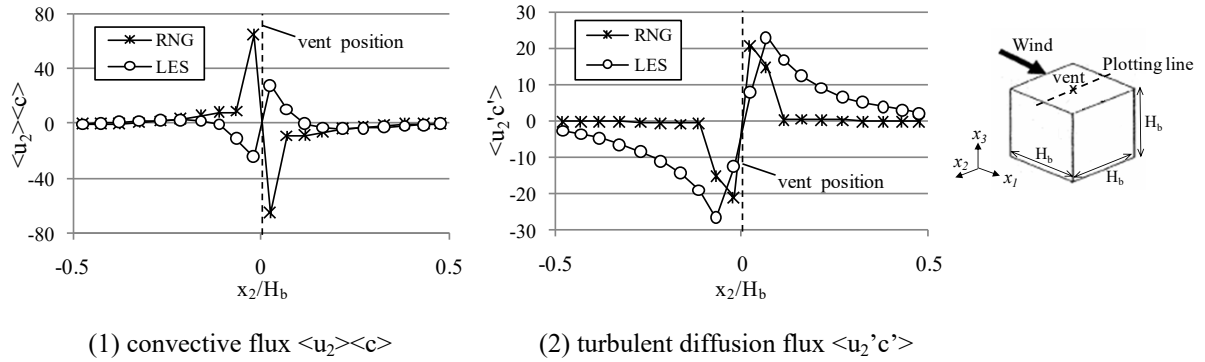
Fig. 12. Comparison of lateral components of convective flux $\langle u_2 \rangle \langle c \rangle$ and turbulent diffusion flux $\langle u_2'c' \rangle$ on roof.

3.5 Concentration fluctuations

When an exhaust gas contains toxic, flammable or odorous components, its instantaneous as well as its average concentrations are of interest. One great advantage of LES is that it can predict fluctuating instantaneous values of concentration. In this study, the concentration fluctuations are normalized by mean concentration magnitudes to give local and absolute intensities by following Li and Meroney [31]. The local intensity Ic ($= \sqrt{\langle c'^2 \rangle} / \langle c \rangle$) is defined as the ratio of the r.m.s. value of the fluctuating concentration to the mean concentration at the same point. The absolute intensity Ic_{abs} ($= \sqrt{\langle c'^2 \rangle} / \langle c_0 \rangle$) is the r.m.s. value of the fluctuating concentration normalized in the same way as the dimensionless concentration, K.

The concentration fluctuation intensity Ic predicted by LES is compared with the experimental data obtained by Li and Meroney [31] in Fig. 13. It should be noted that the flow configurations of two experiments are almost identical, except that the emission velocity ratio in Li and Meroney [31] is a little larger than that in the above-mentioned experiment [16]. However, the predicted values by LES are in good agreement with the experimental data. Fig. 14 (1) shows the concentration distributions of local fluctuation intensity Ic on the roof and the wall surfaces obtained by the present LES computation. At the edge of the cube, very large values of Ic in comparison with those in the center area have been observed. This means that concentration fluctuation is very large compared with the mean concentration at the frontal edge of the cube; the latter was small as shown in Fig. 7. On the other hand, the absolute fluctuation intensity Ic_{abs} indicates a different distribution from Ic as shown in Fig. 14 (2). The distribution of Ic_{abs} is rather similar to that of the mean concentration (cf. Fig. 7), although the region with large values is more spread around the vent position. These properties of the concentration fluctuation are caused by the instantaneous behavior of concentration due to the flapping motion of the plume. Fig. 15 shows the time series of the instantaneous concentration K on the roof and the wall surfaces. Results are presented for different dimensionless time steps t* defined by $\langle u_b \rangle$ and H_b, as mentioned previously. The shapes of the high concentration region vary widely in each time step. These time series assert that the plume dispersion around the building is indeed highly unsteady.
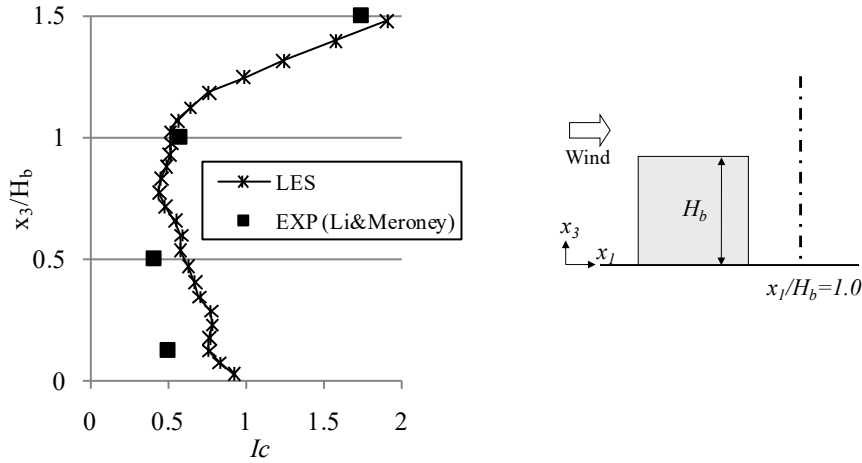
Fig. 13. Concentration fluctuation intensity Ic downstream of cube at centerline.
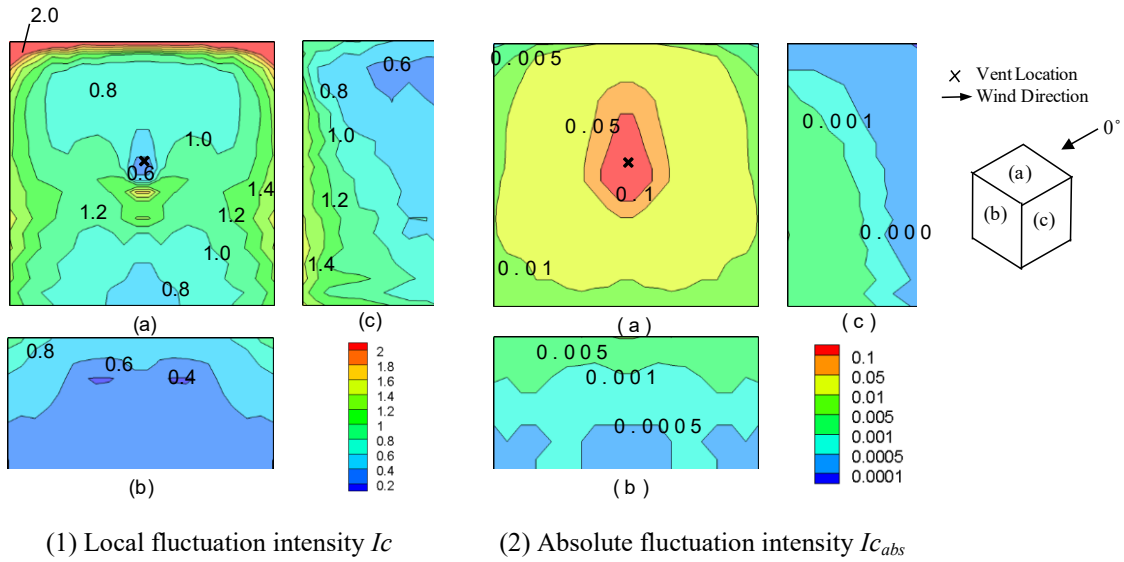

(1) Local fluctuation intensity Ic (2) Absolute fluctuation intensity Ic_{abs}

Fig. 14. Concentration fluctuation intensity Ic on roof and wall surfaces obtained by LES.

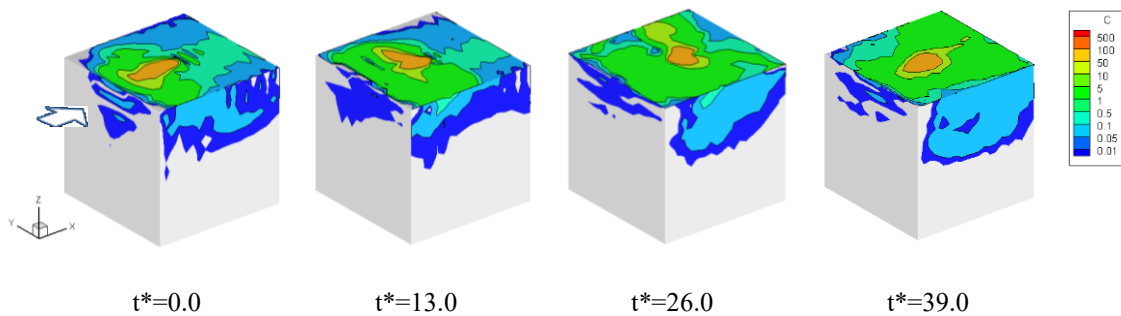t*=0.0   t*=13.0   t*=26.0   t*=39.0

Fig. 15. Time series of instantaneous dimensionless concentration K on roof and wall surfaces obtained by LES.

4   Conclusions

The performance of RANS (RNG) and LES computations was examined for flow and concentration fields around a cube with vent emission in the surface boundary layer. Although more comparisons are needed to end

up with hardy conclusions, the study has contributed in making the following conclusions:

1) LES computation can provide important information on instantaneous fluctuations of concentration, which cannot be obtained by RANS computations.
2) Simple LES modeling gives better results than conventional RANS computation (RNG) modeling of the distribution of concentration, although the difference between LES and RNG results for mean velocity is not so large. The horizontal diffusion of concentration is well reproduced by LES, due mainly to the reproduction of unsteady concentration fluctuations around the cube.
3) RNG underestimates the turbulence diffusion near the cube in comparison with LES. The modeling accuracy of turbulent diffusion is very important for predicting the concentration distribution.
4) Notwithstanding the difficulties to compare directly the computational time of LES and RNG methodologies due to the different convergence criteria between the two methods, the CPU time required to obtain the statistical values in LES is about 25 times longer than that in the RNG case of the present study.

Acknowledgements

References

[1] Li, Y., Stathopoulos, T., 1997. Numerical evaluation of wind-induced dispersion of pollutants around a building. Journal of Wind Engineering and Industrial Aerodynamics 67-68, 757-766.
[2] Meroney, R. N., Leitl, B. M., Rafailidis, S., Schatzmann, M., 1999. Wind-tunnel and numerical modeling of flow and dispersion about several building shapes. Journal of Wind Engineering and Industrial Aerodynamics 81, 333-345
[3] Banks, D., Meroney, R.N., Petersen, R.L. and Carter, J.J., 2003. Evaluation of FLUENT for predicting concentrations on buildings. In: Air and Waste Management Association Annual Conference, San Diego, CA, Paper # 70223.
[4] Tominaga, Y., Stathopoulos, T., 2009. Numerical Simulation of Dispersion around an Isolated Cubic Building : Comparison of Various Types of k-ε Models. Atmospheric Environment 43, 3200-3210.
[5] Blocken, B., Stathopoulos, T., Saathoff, P., Wang X., 2008. Numerical evaluation of pollutant dispersion in the built environment: Comparisons between models and experiments. Journal of Wind Engineering and Industrial Aerodynamics 96, 1817-1831.
[6] Sakamoto, S., Murakami, S., Kato, S., Mochida, A., 1993. Unsteady pressure field around oscillating prism predicted by LES, Journal of Wind Engineering and Industrial Aerodynamics 46-47, 551-556.
[7] Shah, K. B., Ferziger, J. H., 1997. A fluid mechanicians view of wind engineering: Large eddy simulation of flow past a cubic obstacle, Journal of Wind Engineering and Industrial Aerodynamics 67-68, 211-224.
[8] Tamura, T., Ono, Y., 2003. LES analysis on aeroelastic instability of prisms in turbulent flow, Journal of Wind Engineering and Industrial Aerodynamics 91, 1827-1846.
[9] Murakami, S., 1993. Comparison of various turbulence models applied to a bluff body. Journal of Wind Engineering and Industrial Aerodynamics 46-47, 21-36.
[10] Rodi, W., 1997, Comparison of LES and RANS calculations of the flow around bluff bodies. Journal of Wind Engineering and Industrial Aerodynamics 69-71, 55-75.
[11] Tominaga, Y., Mochida, A., Murakami, S., Sawaki, S., 2008. Comparison of various revised k-ε models and LES applied to flow around a high-rise building model with 1:1:2 shape placed within the surface boundary layer. Journal of Wind Engineering and Industrial Aerodynamics 96, 389-411.
[12] Li, X.-X., Liu, C.-H., Leung, D. Y. C., Lam, K. M., 2006. Recent progress in CFD modelling of wind field and pollutant transport in street canyons. Atmospheric Environment 40, 5640-5658.
[13] Tamura, T., 2008, Towards practical use of LES in wind engineering, Journal of Wind Engineering and Industrial Aerodynamics 96, 1451-1471.
[14] Tominaga, Y., Murakami, S., Mochida, A., 1997. CFD Prediction of Gaseous Diffusion around a Cubic Model using a Dynamic Mixed SGS Model based on Composite Grid Technique. Journal of Wind Engineering and Industrial Aerodynamics 67-68, 827-841.
[15] Sada, K., Sato, A., 2002. Numerical calculation of flow and stack-gas concentration fluctuation around a cubical building, Atmospheric Environment 36, 5527-5534.
[16] Li, W.-W., Meroney, R. N., 1983a. Gas dispersion near a cubical model building, Part I, Mean concentration measurements. Journal of Wind Engineering and Industrial Aerodynamics 12, 15-33.
[17] Brzoska, M. A., Stock, D., Lamb, B., 1997. Determination of plume capture by the building wake, Journal of Wind Engineering and Industrial Aerodynamics 67-68, 909-922.

[18] Olvera, H. A., Choudhuri, A. R., Li, W.-W., 2008. Effects of plume buoyancy and momentum on the near-wake flow structure and dispersion behind an idealized building, Journal of Wind Engineering and Industrial Aerodynamics 96, 209-228.

[19] Nakiboğlu, G., Gorlé, C., Horváth, I., van Beeck, J., Blocken, B., 2009. Stack gas dispersion measurements with Large Scale-PIV, Aspiration Probes and Light Scattering Techniques and comparison with CFD, Atmospheric Environment 43, 3396-3406.

[20] Yakhot, V., Orszag, S.A., Thangam, S., Gatski, T.B., Speziale, C.G., 1992. Development of turbulence models for shear flows by a double expansion technique. Physics of Fluids A4, 1510–1520.

[21] Tominaga, Y. and Stathopoulos, T., 2007. Turbulent Schmidt numbers for CFD analysis with various types of flowfield. Atmospheric Environment 41, 8091-8099.

[22] Smagorinsky, J., 1963. General circulation experiments with the primitive equations I. The basic experiment. Monthly Weather Review 91, 99-164.

[23] Germano, M., Piomelli, U., Moin, P., Cabot, W.H., 1991. A dynamic subgrid-scale eddy viscosity model. Physics of Fluids A3, 1760-1765.

[24] Iizuka, S., Kondo, H., 2004. Performance of various sub-grid scale models in large-eddy simulations of turbulent flow over complex terrain. Atmospheric Environment 38, 7083-7091.

[25] Antonopoulos-Domis, M., 1981. Large eddy simulation of a passive scalar in isotropic turbulence, Journal of Fluid Mechanics 104, 55–79.

[26] Launder, B.E., Spalding, D.B., 1974. The numerical computation of turbulent flows. Comput. Methods Appl. Mech. Eng. 3, 269–289.

[27] Kataoka, H., Mizuno, M., 2002. Numerical flow computation around aeroelastic 3D cylinder using inflow turbulence, Wind and Structures 5, 379-292.

[28] Ono, Y., Tamura, T., Kataoka, H., 2008. LES analysis of unsteady characteristics of conical vortex on a flat roof, Journal of Wind Engineering and Industrial Aerodynamics 96, 2007-2018.

[29] Werner, H., Wengle, H., 1993. Large Eddy Simulation of Turbulent Flow over and around a Cube in Plane Channel. In : Proceedings of 8th Symposium on Turbulent Shear Flows, 155-168.

[30] Saathoff, P.J., Stathopoulos, T., Dobrescu, M., 1995, Effects of model scale in estimating pollutant dispersion near buildings, Journal of Wind Engineering and Industrial Aerodynamics 54-55, 549-559.

[31] Li, W.-W., Meroney, R. N., 1983b. Gas dispersion near a cubical model building, Part II, Concentration fluctuation measurements. Journal of Wind Engineering and Industrial Aerodynamics 12, 35-47.